Ⓔ

Strong-Motion Observations of the Lushan Earthquake on 20 April 2013

by Ruizhi Wen and Yefei Ren

Online Material: Additional figures of acceleration time series; table of station parameters, associated ground motion intensities.

INTRODUCTION

On 20 April 2013, at 08:02 a.m. Beijing time, a strong earthquake hit Lushan, a county in the southwest of Sichuan Province in China. During this earthquake, a total of 114 strong-motion stations from the new generation of the National Strong-Motion Observation Network System (NSMONS) of China were triggered. The NSMONS consists of 1154 permanent free-field stations and began to operate in March 2008. The 2008 Wenchuan destructive earthquake triggered a large number of strong-motion recordings that contribute significantly to the world strong-motion database (Li, Zhou, Huang, *et al.*, 2008). The 2013 Lushan earthquake also provided a large number of near-source recordings in China (Xie *et al.*, 2014).

NSMONS aims to enhance the ability of earthquake monitoring and the collection of strong-motion recordings in the most seismically active regions and some major cities in the Chinese mainland. As a result, its free-field stations are irregularly distributed with an average spacing of 50 km to hundreds of kilometers (Li, Zhou, Yu, *et al.*, 2008). Thus, it definitely cannot monitor all of the seismic areas in China. For example, on 14 April 2010, the Yushu earthquake, which exhibited a magnitude of M_s 7.1, occurred in the northeast part of the Tibetan plateau at Yushu, Qinghai Province. Only five strong-motion stations of NSMONS were triggered, the nearest of which was approximately 350 km from the epicenter, and the maximum peak ground acceleration (PGA) was only approximately 2 cm/s^2. Taking into account the randomness of the spatial distribution of earthquakes, most strong-motion recordings obtained in recent years have small amplitudes and are thus not of interest to engineers (China Strong Motion Networks Center, 2012). As a result, these recordings only contribute to the steady growth of the strong-motion database rather than to systematic studies of earthquake engineering and seismology. A large number of near-fault high-amplitude strong-motion recordings from the Lushan earthquake would provide an excellent opportunity for further studies.

In this paper, we present an overview of the strong-motion observations from the Lushan earthquake. The characteristics of the strong-motion recordings at near-field and far-field sites are preliminarily analyzed. The differences between the horizontal PGAs on the hanging wall and footwall are evaluated by regressing a simple attenuation model based on the recordings within a rupture distance of 200 km. The observed PGAs, peak ground velocities (PGVs), and spectral accelerations are compared with the predicted values given by the widely used ground-motion prediction equations (GMPEs) in China and the Next Generation Attenuation (NGA-West2) model developed by Boore *et al.* (2013), which is hereafter referred to as BSSA2013. The potential topographic effect on some near-field recordings is also inferred.

THE 20 APRIL 2013 LUSHAN EARTHQUAKE SEQUENCE

The Lushan earthquake occurred on the southern segment of the Longmenshan thrust belt, which is considered an area with relatively high seismic risk between Bayan Har and south China blocks. This earthquake sequence is another destructive event following the 2008 Great Wenchuan earthquake. A magnitude of M_s 7.0 for the mainshock was estimated by the China Earthquake Networks Center, and a magnitude of M_w 6.6 was estimated by the U.S. Geological Survey (USGS). The rupture process was inversed by Wang *et al.* (2013) using the regional broadband waveforms; the results show the calculated moment magnitude M_w was 6.7, and the strike, dip, and slip angles were 205°, 38.5°, and 88.8°, respectively. The seismogenic fault is a reversed one, and two subevents are included with the largest slip of approximately 159 cm. From the spatial epicenter locations of the Lushan and Wenchuan earthquake sequences, Xu *et al.* (2013) found that both the Wenchuan and Lushan earthquakes occurred on the same fault belt but on the north and south segments, respectively and that the distance between the epicenters of both mainshocks was 90 km. These researchers noted the two earthquakes could be considered independent rupturing events because, assuming the spatial distribution of the aftershocks represents the plane of rupture, there was no overlap between the two focal ruptures of the Wenchuan and Lushan earthquakes.

By the end of 27 April 2013, approximately 3811 aftershocks occurred, and most of these occurred were in a 35 km long and 16 km wide area in Baoxing, Qionglai, Lushan, and Tianquan Counties (Fang *et al.*, 2013), which is consistent

doi: 10.1785/0220140006

with the fault rupture plane reported by Wang *et al.* (2013). To record as many aftershocks as possible, seven temporal strong-motion stations were installed around the epicenter area on the day following the mainshock. Until 6 July 2013, a total of 1123 strong-motion recordings were obtained from NSMONS and the 7 temporal stations. The maximum PGA from the aftershocks is 576 cm/s^2, as recorded by the 51LSJ station at 11:59:02 a.m. (local time) on 21 April 2013.

OBSERVED STRONG-MOTION RECORDINGS

Overview of Recordings

During the mainshock, 121 digital strong-motion instruments of NSMONS were triggered, among which 114 ones were at free-field sites and 7 served as a structural observation array in the city of Kunming, which is 600 km away from the epicenter.

An additional 63 stations from the Local Seismic Intensity Reporting Network of the city of Chengdu, the capital city of Sichuan Province, were triggered. This local network, which was built after the 2008 Wenchuan earthquake, consists of 80 free-field strong-motion stations. The local network stations transmit data in real time; therefore, the instrumental intensity could be easily calculated if an event occurs. The Earthquake Disaster Prevention Bureau of Chengdu is responsible for its operation, data collection, and dissemination. It is the first time the local network could provide such a large number of strong-motion recordings to the public. All of the triggered stations of the two networks are shown in Figure 1, and these stations cover parts of Sichuan, Yunnan, Gansu, and Shanxi Provinces in China.

For the national network, most of the accelerometers are ETNA and MR2002 models, and the full range is $\pm 2g$ with a sampling rate of 200 samples/s. For the local network, all of the accelerometers are the TAIDE model (made in China), and the full range is $\pm 2g$ with a sampling rate of 100 samples/s. As is well known, there is no panacea that can be prescribed for the data processing of strong-motion recordings. Different signal processing techniques affect the resulting ground-motion time histories in different ways. In China, both the national and local networks only provide the digitized data after a zeroth-order correction by removing the pre-event mean from the whole recording. The end users can choose their own optimal processing procedure depending on the application. The strong-motion recordings in the present study are processed using the same methodology that was applied for the Wenchuan earthquake (Boore, 2001; Ren *et al.*, 2011). The baseline correction was made for some near-field recordings, and then a Butterworth filter with a 0.05–50 Hz bandwidth was applied. As a result, the processed ground motion can be considered to provide reliable estimates of PGA, PGV, peak ground displacement (PGD), and the spectral ordinates that interest the engineers (Ⓔ Table S1, available as an electronic supplement to this article). Ⓔ To provide useful information for comparisons with GMPEs, the epicenter distance (R_{epi}), Joyner–Boore distance (R_{JB}), and rupture distance (R_{rup}) are also listed in Table S1.

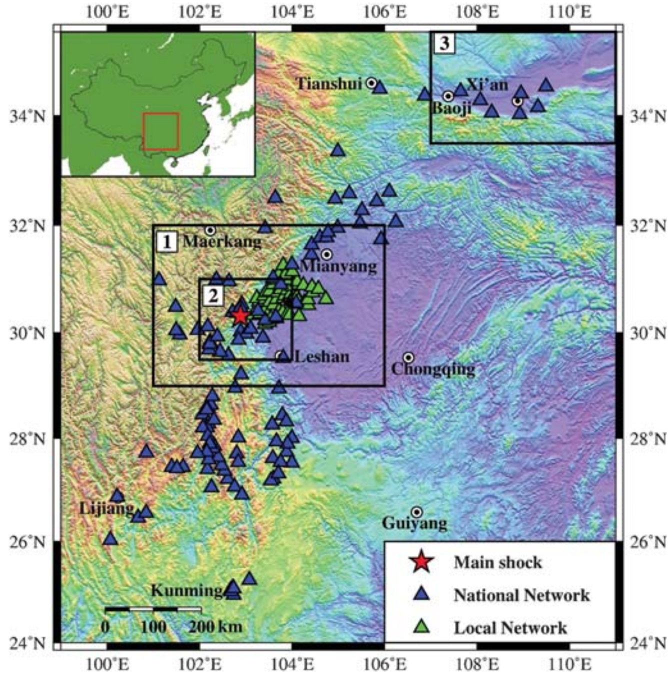

▲ **Figure 1.** Triggered strong-motion stations during the Lushan earthquake mainshock. The blue triangles indicate the stations of the National Strong-Motion Observation Network System (NSMONS). The green triangles show the stations of the Local Seismic Intensity Reporting Network of Chengdu, which exhibit a dense distribution around the city of Chengdu. Boxes 1, 2, and 3 bound the areas shown in Figures 2, 3a, and 4a.

There are 171 components with PGA values less than 10 cm/s^2, 214 components with PGA values ranging from 10 to 50 cm/s^2, 78 components with PGA values ranging from 50 to 100 cm/s^2, 39 components with PGA values ranging from 100 to 200 cm/s^2, 22 components with PGA values ranging from 200 to 400 cm/s^2, and 7 components with PGA values greater than 400 cm/s^2. The contour maps of PGA and PGV in the east–west (EW), north–south (NS), and up–down (UD) directions are interpolated using the Kriging interpolation method, as shown in Figure 2. To make the contours clearer, we use the natural logarithm of the ground motion, and the results show that the PGA and PGV were attenuated faster in the mountainous area than in the plain area, Sichuan basin, perhaps indicating the entrapment and amplification of seismic waves by deep sediments. The interpolation may be very sensitive to some unique sites lying in the basin interior, and we attempted to exclude some to make the interpolation and contour maps continue to show the same trend.

Observed Near-Field Strong-Motion Recordings

There are 79 strong-motion stations located within an R_{rup} of 100 km, 13 of which are located within 20 km. Figure 3 shows the locations of these 13 stations and two additional stations with large PGAs. The acceleration time histories obtained from 5 hanging-wall stations are plotted in Figure 3, and those from the other 10 stations are plotted in Ⓔ Figure S1.

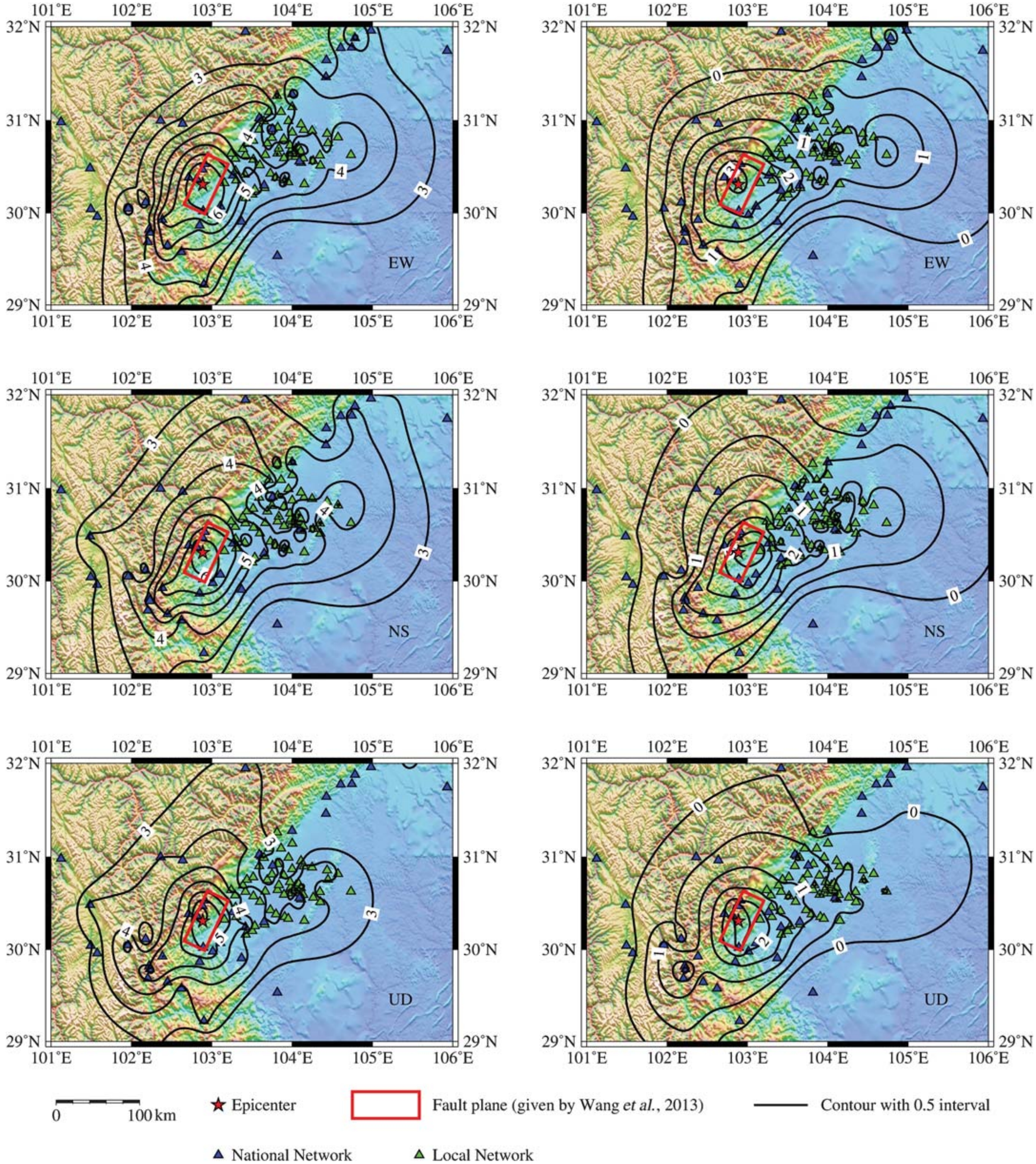

▲ **Figure 2.** Contour maps of the natural logarithm of (left) the peak ground acceleration (PGA in cm/s^2) and (right) peak ground velocity (PGV in cm/s) values in the east–west (EW; top), north–south (NS; middle), and up-down (UD; bottom) components for the Lushan earthquake. The area is shown in Figure 1 as box 1.

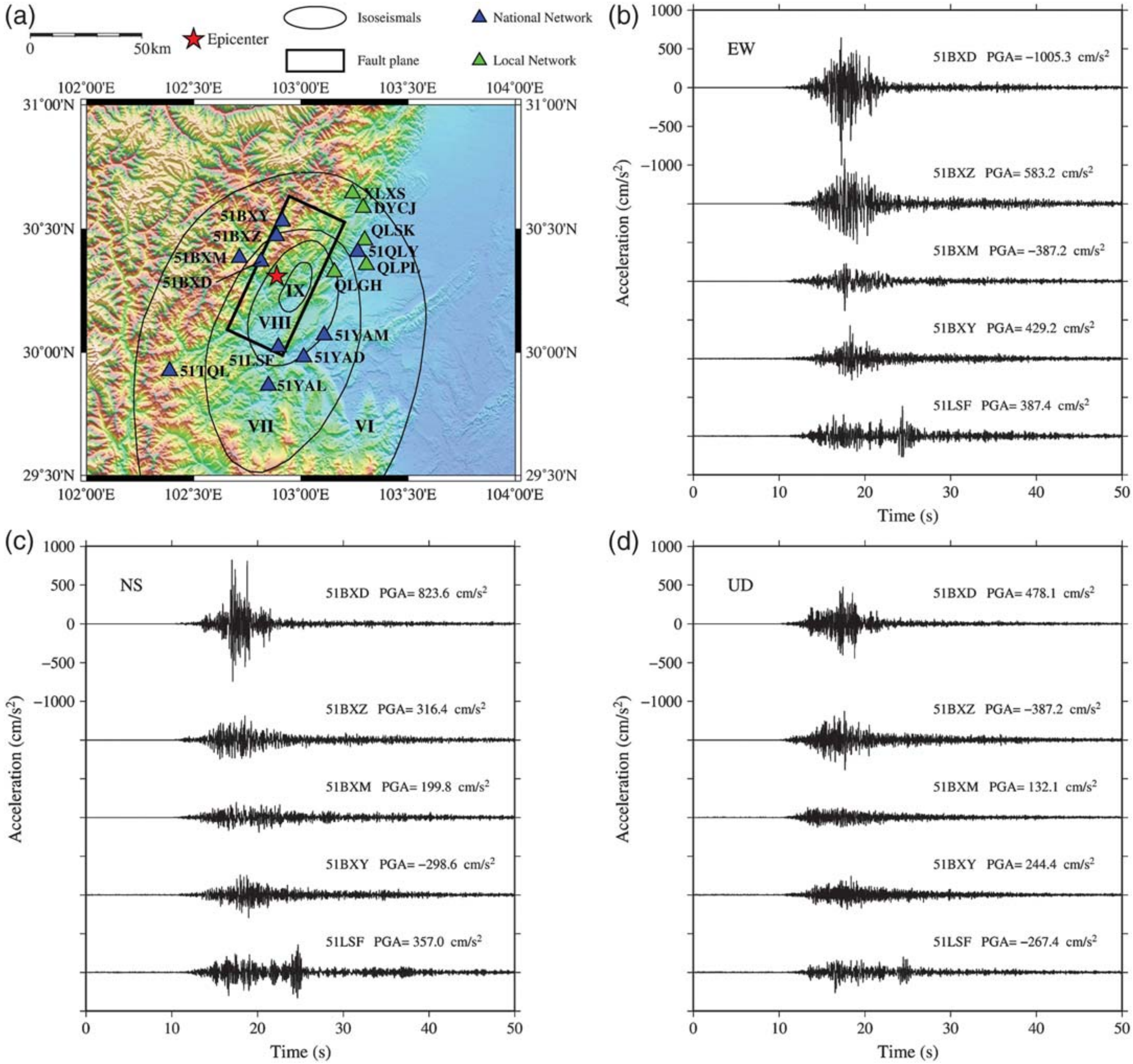

▲ **Figure 3.** (a) Locations of the near-field strong-motion stations ($R_{\rm rup}$ < 20 km) and two additional stations that recorded large PGA values during the Lushan earthquake and acceleration time-histories for the (b) EW, (c) NS, and (d) UD components at the five hanging-wall sites shown in Figure 8a. The rectangle shown in (a) is the projection of the rupture plane on the surface given by Wang *et al.* (2013). The isoseismals are digitized from the macroseismic intensity map released by the China Earthquake Administration. A larger-scale map of the area is also shown in Figure 1 as box 2.

The largest PGA was observed at the 51BXD station in Baoxing County, which recorded PGAs in the EW, NS, and UD directions of −1005.3, 823.6, and 478.1 cm/s^2, respectively. This is the first recording of PGA values exceeding 1g (i.e., 981 cm/s^2) in Chinese strong-motion observation history. Even for the 2008 Wenchuan earthquake, the maximum PGAs recorded at the Wolong station did not exceed 1g (957.7, 652.9, and 948.1 cm/s^2 in the EW, NS, and UD directions, respectively). The second largest recording was obtained at the 51BXZ station in Baoxing County, with PGAs in EW, NS, and UD directions of 583.2, 316.4, and −387.2 cm/s^2, respectively.

Observed Far-Field Strong-Motion Recordings

The potential impact of far-source long-period ground motion was first recognized worldwide in the Michoacan earthquake in 1985 (Celebi *et al.*, 1987). The Weihe basin is located in Shanxi Province, approximately 700 km from the epicenter of

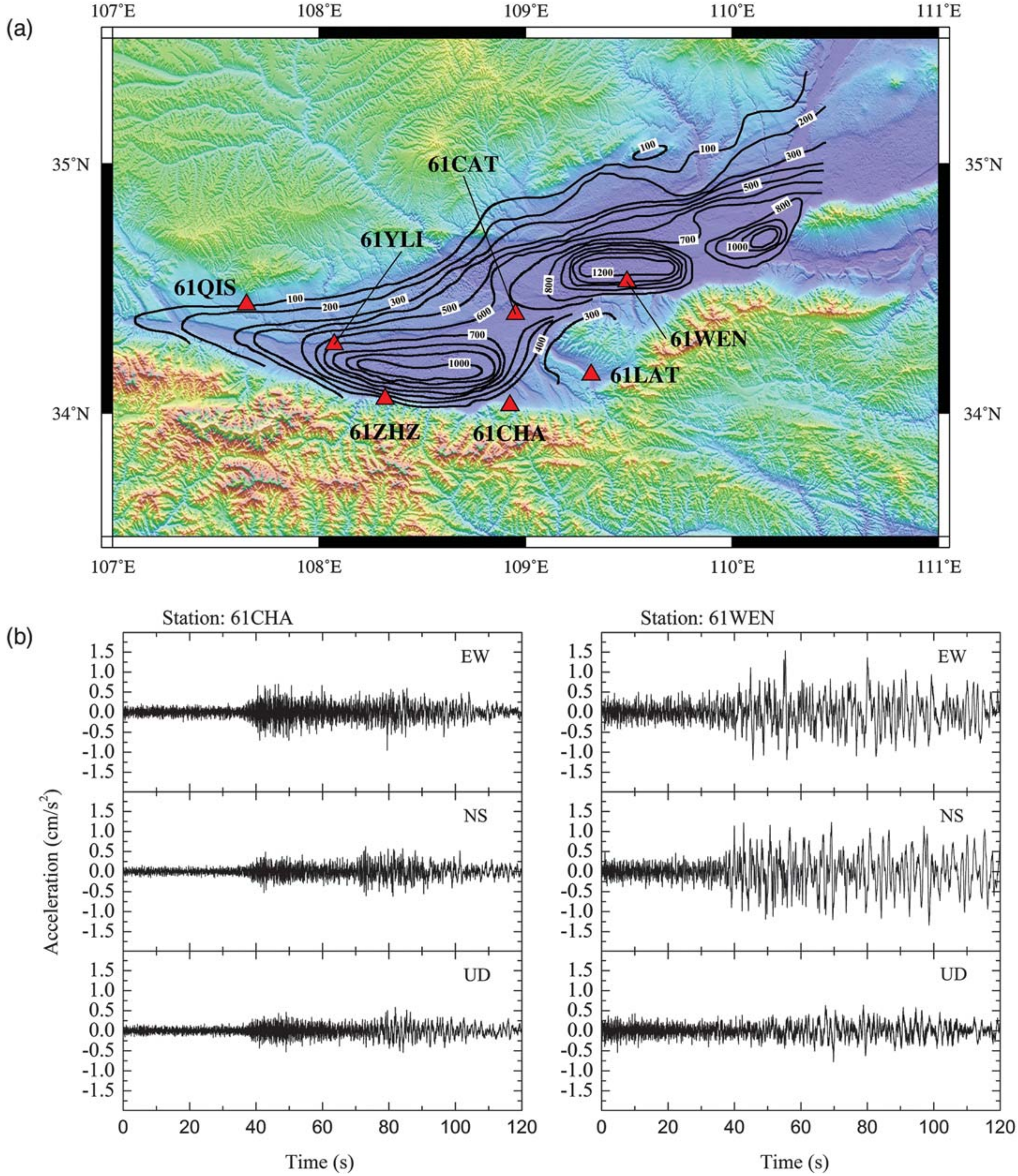

▲ **Figure 4.** (a) Locations of the seven triggered strong-motion stations in the Weihe basin. The contours of constant Quaternary sediment thickness with a 100 m interval (Peng, 1992) are shown as black lines. A large-scale map of the area is also shown in Figure 1 as box 3. (b) Typical acceleration time histories observed at (left) a rock site and (right) a soil site.

Table 1
The Ground Motion Parameters of Some Far-Field Strong-Motion Recordings Observed in the Weihe Basin

Station Code	Longitude (°)	Latitude (°)	Site Condition	Epicenter Distance (km)	PGA (cm/s^2) EW	PGA (cm/s^2) NS	PGA (cm/s^2) UD
61CAT	108.95	34.40	Soil	728.3	2.77	−2.67	0.80
61CHA	108.92	34.03	Rock	702.3	−0.95	0.63	0.59
61LAT	109.32	34.15	Soil	740.0	1.49	1.18	0.59
61QIS	107.65	34.44	Soil	640.4	−2.16	−1.90	1.37
61WEN	109.49	34.53	Soil	776.6	1.53	−1.34	−0.78
61YLI	108.07	34.28	Soil	656.9	2.51	−2.74	1.05
61ZHZ	108.32	34.06	Soil	659.2	1.57	1.65	1.15

Lushan earthquake (box 3 in Fig. 1). During the 2008 Wenchuan earthquake, two abnormal regions of macroseismic intensities VI and VII were identified based on the postearthquake investigation in this basin area. Significant site amplification is caused by the deep Quaternary sediment layers, as shown by the results of the application of the standard spectral ratio (SSR) method to the strong-motion recordings in the basin (Wang, 2011).

With regard to the Lushan earthquake, seven stations recorded the event within the basin. Figure 4a shows the locations of these stations and the isolines of the thickness of quaternary sediment layers given by Peng (1992), the maximum depth of which is greater than 1200 m. The geographic coordinates, site conditions, epicenter distances, and observed PGAs for each station are listed in Table 1. The far-field long-period ground motions could consist of surface waves excited by the path and site effects. Figure 4b shows the acceleration time histories recorded at stations 61CHA and 61WEN, which are classified as rock and soil sites, respectively. Because both are more than 700 km from the epicenter, the 20 s of pre-event time setting is not long enough to record the *P*-wave arrival. The amplitudes of the two horizontal components at station 61WEN were larger than those at 61CHA and contain more long periods. Their approximate epicenter distances indicate the path effects should be very similar; therefore, it could be understandable that the thick soil deposit has a considerable effect on the ground motion.

We use the SSR method and station 61CHA as the reference site to analyze the site effect for each of the other six soil sites based on the mainshock recordings following the methodology proposed by Ren, Wen, *et al.* (2013). The *S*-wave window is extracted and tapered, and the geometric mean of the two horizontal components of the Fourier amplitude spectrum is computed. The calculated spectral ratios for each site are presented in Figure 5, which shows amplifications in the period ranges of 0.4–0.9 s, 1.1–1.5 s, 2.3–3.0 s, and 7.0–9.0 s.

Station 61WEN, which is located in the middle of the basin and has sedimentary layers with a thickness of approximately 1000 m, is the only station that clearly shows two long-period peaks. Stations 61CAT and 61YLI also show a long-period peak at approximately 8.0 s and a wide amplification in the 0.25–3.0 s band, with larger peaks at 1.2 and 2.5 s. Both of these stations are also located in the middle of the basin and have deposit layers with thicknesses of approximately 700 m. Surprisingly, 61LAT shows a single clear peak at 2.8 s, and this station seems to be located outside the basin (or at the border). 61QIS and 61ZHZ, which are near the border of the basin, show amplification at 0.4–0.9 s, and 61QIS also shows amplification at 1.2 s. Therefore, at sites with thicker deposits, the amplification appears at longer periods, which is consistent with a site effect induced by sediment thickness. Of course, a basin-edge effect, in addition to the amplification linked to a deep sediment layer, can also affect the data. It is worth noting that more recordings from more events are needed to obtain an SSR shape with good stability, and the above descriptions only show a specific result for the mainshock of Lushan earthquake.

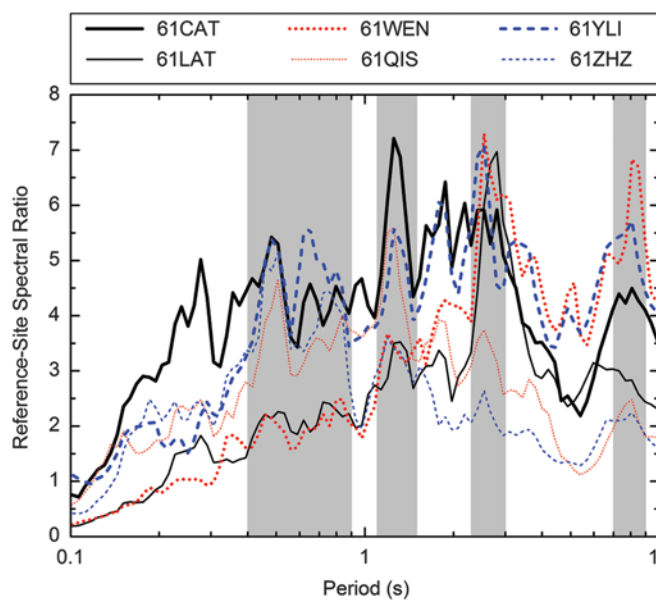

▲ **Figure 5.** Reference-site spectral ratios for the six soil sites in the Weihe basin using the rock site 61CHA as reference. The shaded areas show period ranges at which amplification peaks are observed.

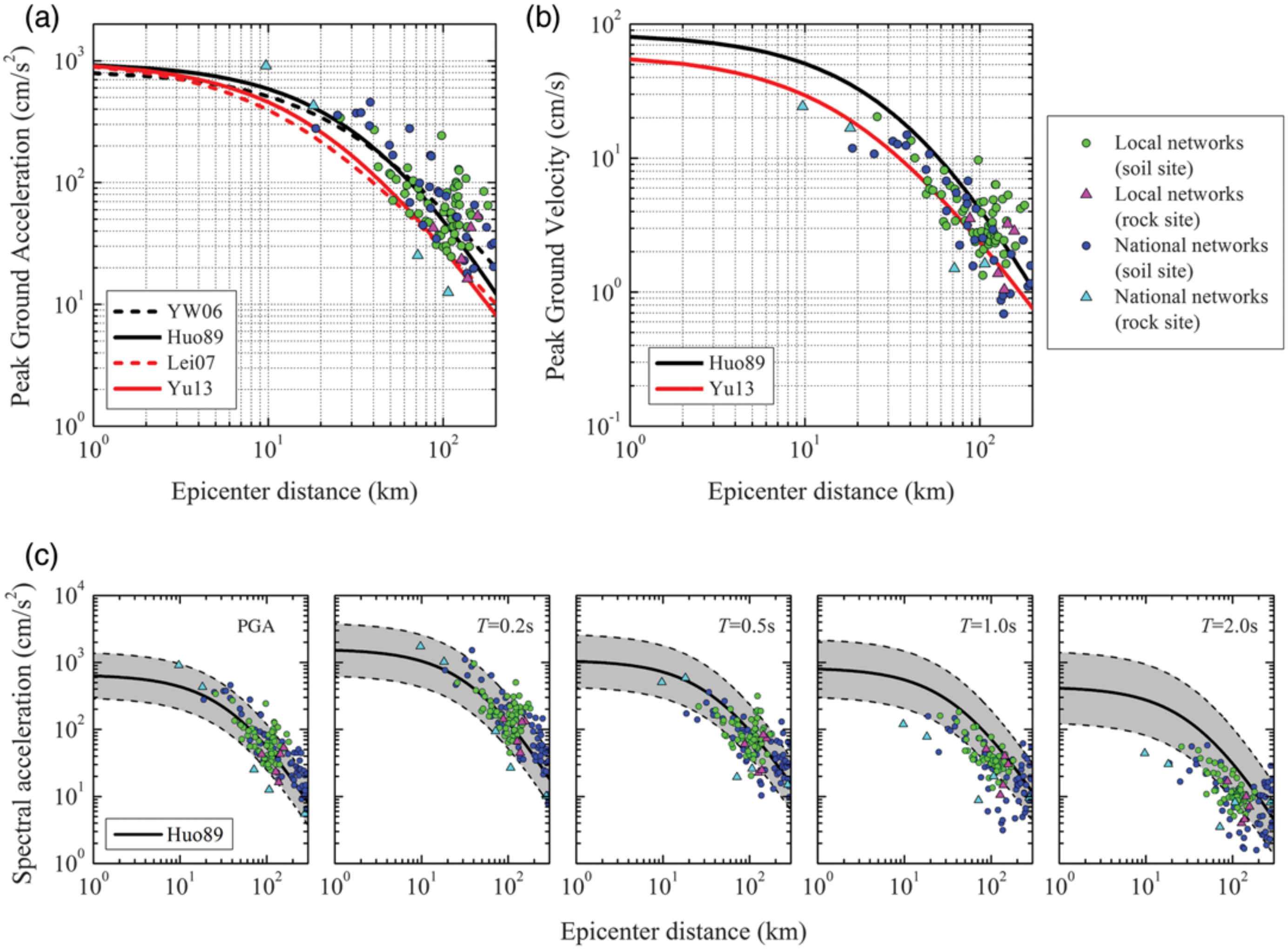

▲ **Figure 6.** Comparison between the observed and predicted horizontal median (a) PGAs and (b) PGVs. The predicted median values were calculated using four popular Chinese ground-motion prediction equations (GMPEs) for rock sites. (c) Comparison between the observed and predicted horizontal PGAs and 5% damped spectral accelerations at periods $T = 0.2$, 0.5, 1.0, and 2.0 s. The predicted median values were calculated using Huo (1989) for soil sites. The shaded area denotes the ± 1 standard deviation range.

Comparison with GMPEs

The observed horizontal PGAs and PGVs were compared with some popular GMPEs in China (Fig. 6a,b): YW06 for western China (Yu and Wang, 2006), Huo89 for southwest China (Huo, 1989), Lei07 for the Sichuan basin (Lei *et al.*, 2007), and Yu13 for the fifth-generation Chinese seismic zonation map (Yu *et al.*, 2013). All of these were developed using a transform method proposed for regions with no ground-motion data (Hu and Zhang, 1983). This method assumes that region A has enough historical macroseismic intensity data and enough ground-motion data, whereas region B has enough historical macroseismic intensity data but little ground-motion data. The major goal is to build a ground-motion attenuation relationship in region B by mapping two sets of intensity attenuation curves from both regions A and B. These GMPEs are applicable for the epicenter distances lower than 200 km, and the Huo89 GMPE is applicable for distances lower than 300 km. The ground-motion parameters include the PGA and the 5% damped pseudoresponse spectral acceleration (PSA) at periods from 0.04 to 6.0 s for YW06 and Lei07, the PGA, PGV, PGD, and PSA at periods from 0.04 to 8.0 s for Huo89, and only the PGA and PGV for Yu13. The magnitude ranges from 5.0 to 8.0 for YW06 and Huo89, from 5.0 to 7.0 for Lei07, and from 4.5 to 8.0 for Yu13. The rock and soil site conditions are included in Huo89, and only the rock site condition is included in the other three GMPEs.

When the predicted PGAs are calculated, the rock site condition is considered for Huo89 GMPE in order to maintain consistency with the other three GMPEs, YW06, Lei07, and Yu13 which are only available for rock sites. Figure 6a shows the median PGA values predicted by Yu13 and Lei07 are lower than the observed values for the whole distance range with two exceptions. Those values predicted by Huo89 and YW06 seem closer to the observed data. Because the GMPEs are used for rock conditions and most of the data are soil sites, the apparent discrepancy could be attributed to site effects. The two points

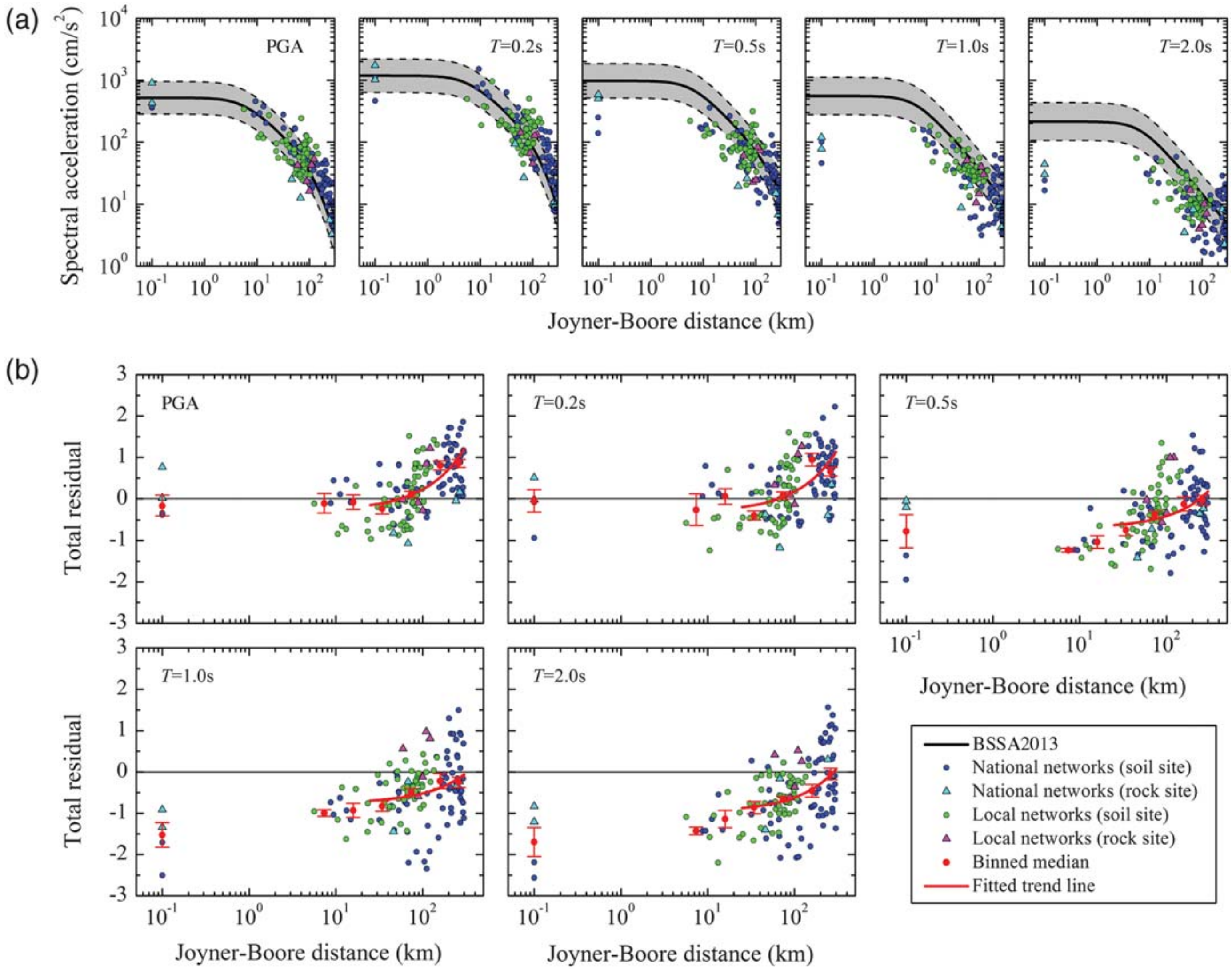

▲ **Figure 7.** (a) Comparison between the observed and predicted horizontal PGAs and 5% damped spectral accelerations at periods $T = 0.2$, 0.5, 1.0, and 2.0 s. The predicted values were calculated using the GMPE developed by Boore *et al.* (2013) with $V_{S30} = 350$ m/s. The shaded area denotes the ±1 standard deviation range. (b) Residuals between the observed and predicted values calculated assuming $V_{S30} = 350$ m/s for soil sites and $V_{S30} = 760$ m/s for rock sites. Binned values with respect to distance are also shown (red dots; the bars indicate the standard errors). Note that the data points with R_{JB} less than 0.1 km are plotted at 0.1 km.

with the lowest PGAs are two rock sites. For PGVs, the median values predicted by Huo89 and Yu13 pass through the data, but the near-field data (distance lower than 20 km) predicted by Huo89 are slightly higher than the few observed data.

The observed horizontal PSAs with 5% damping ratio are also compared with the predicted values from Huo89 in terms of soil site for periods $T = 0.0$ (i.e., PGA), 0.2, 0.5, 1.0, and 2.0 s (Fig. 6c). Considering the fact that most of observed values are obtained from soil sites, the soil site condition is chosen for calculating the predicted values. The observed PGAs and PSAs at short and medium periods of 0.2 and 0.5 s are within one standard deviation from the predicted values. However, for longer periods of 1.0 and 2.0 s, the GMPEs overpredict the data.

Figure 7 presents a comparison between the observed PGAs and PSAs with the GMPE developed by BSSA2013. The data observed within $R_{JB} = 300$ km are used (Ⓔ Table S1). We assume an average uppermost 30 m shear-wave velocity (V_{S30}) of 350 m/s represents soil sites around the Lushan area (Wang *et al.*, 2010), and 760 m/s was used for rock sites.

For PGAs and PSAs at $T = 0.2$ s, most of the observed values are consistent with the predicted values within $R_{JB} = 100$ km, while many of the observed values are beyond one standard deviation away from the predicted values when R_{JB} is greater than 100 km, implying that the BSSA2013 results in underpredictions (Fig. 7a). The residuals are calculated based on $V_{S30} = 350$ m/s for soil sites and $V_{S30} = 760$ m/s for rock sites, because the individual V_{S30} are unknown. Figure 7b shows the residuals between the observed and predicted values demonstrate an increasing trend with increasing

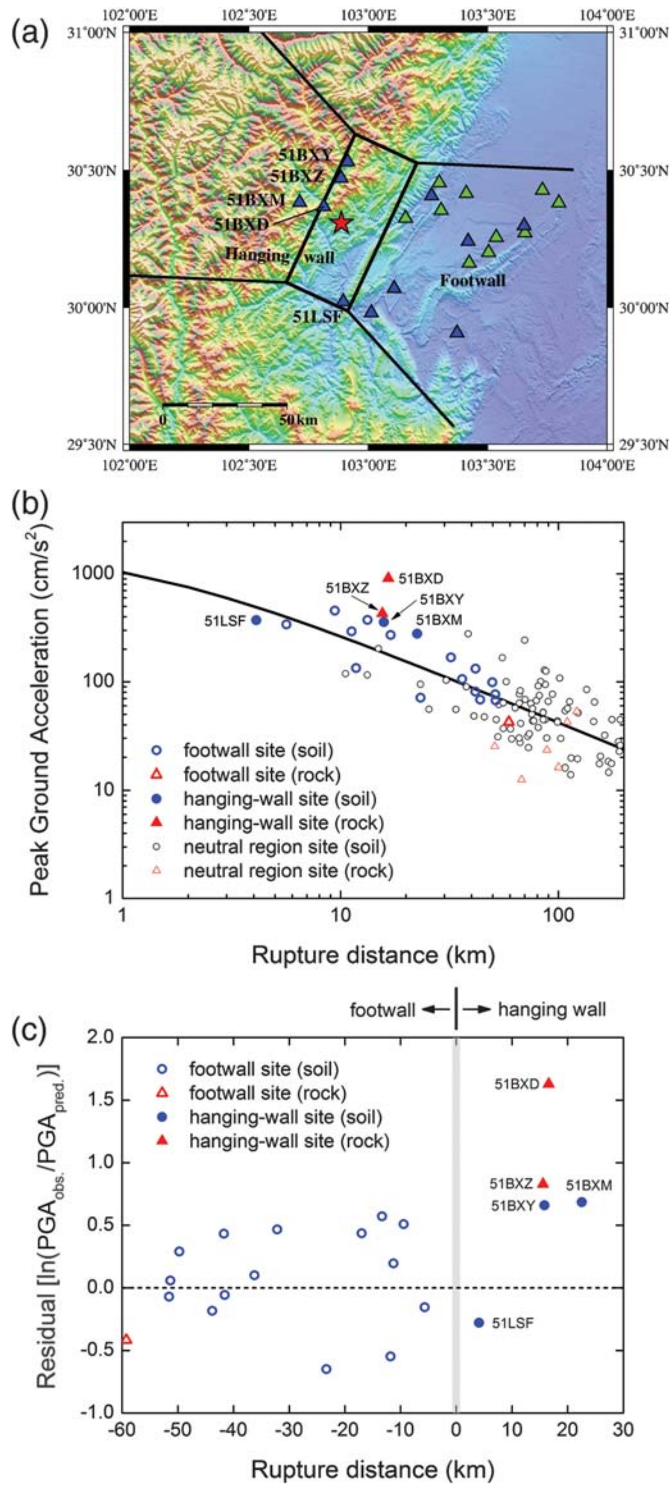

▲ **Figure 8.** (a) Delineation of the hanging-wall and footwall regions in the Lushan earthquake according to the definition suggested by Abrahamson and Somerville (1996) and the fault rupture plane reported by Wang *et al.* (2013). The strong-motion stations located within these two regions are shown as blue triangles (national network stations) and green triangles (local network stations). (b) Empirical attenuation model of horizontal PGA regressed from equation (1). (c) Residuals of regressed model plotted as a function of rupture distance for each hanging-wall and footwall site in (a).

Table 2
Regression Coefficients Used in Equation (1) to Estimate PGA in the Lushan Earthquake

a	b	c	$\sigma_{\ln Y}$
7.583	−0.833	1.158	0.349

distance, thereby exhibiting low-anelastic attenuation (i.e., high Q) in the Lushuan region, as was also observed by Boore *et al.* (2013) for the 2008 Wenchuan earthquake data. A majority of the observed PSAs at $T = 0.5$, 1.0, and 2.0 s are lower than the median values predicted by BSSA2013 within $R_{\mathrm{JB}} = 100$ km as shown in Figure 7a, resulting in mostly negative residuals (Fig. 7b). It implies a low between-event residual for Lushan earthquake, as was also observed by Boore *et al.* (2013) for the other Chinese events.

Hanging-Wall Effect

The ground motions from the thrust earthquakes are likely to show a systematic difference between the hanging wall and footwall. Usually, it is larger on a hanging-wall site than on a footwall site, even though both have the same rupture distances (Abrahamson and Somerville, 1996). Figure 8a outlines the regions of hanging wall and footwall in the Lushan earthquake according to the definition given by Abrahamson and Somerville (1996) and the fault rupture plane reported by Wang *et al.* (2013). There are 5 stations located within the hanging-wall region, namely 51BXD, 51BXM, 51BXY, 51BXZ, and 51LSF, and 16 stations within the footwall region (Ⓔ Table S1). The acceleration time histories recorded from these five hanging-wall stations are plotted in Figure 3. By studying the hanging-wall effect in the Lushan earthquake, we developed a simplified ground-motion model based on the recordings with a rupture distance of less than 200 km (Ⓔ Table S1). The functional form is given by

$$\ln Y = a + b \ln(R_{\mathrm{rup}} + c), \quad (1)$$

in which Y is the geometrical mean of the PGA values observed in the two horizontal components (in cm/s^2), and the coefficients a, b, and c are derived from the regression based on the least-square method together with the standard deviation $\sigma \ln Y$ of the regression. The values of these parameters are listed in Table 2. This equation was used to evaluate the hanging-wall effect on ground motion in the Chi-Chi earthquake (Chang *et al.*, 2004) and the Wenchuan earthquake (Liu and Li, 2009).

The corresponding median curve of PGA is compared with the observed data in Figure 8b. In this figure, all of the observed PGAs for the hanging-wall sites, with the exception of that for 51LSF, are above the regressed median curve, whereas those for the footwall sites exhibit a normal distribution. The regressed residuals range from approximately 0.6 to 0.6 for the footwall sites, but four of the five hanging-wall sites exhibit residuals greater than 0.6, as shown in Figure 8c. In particular,

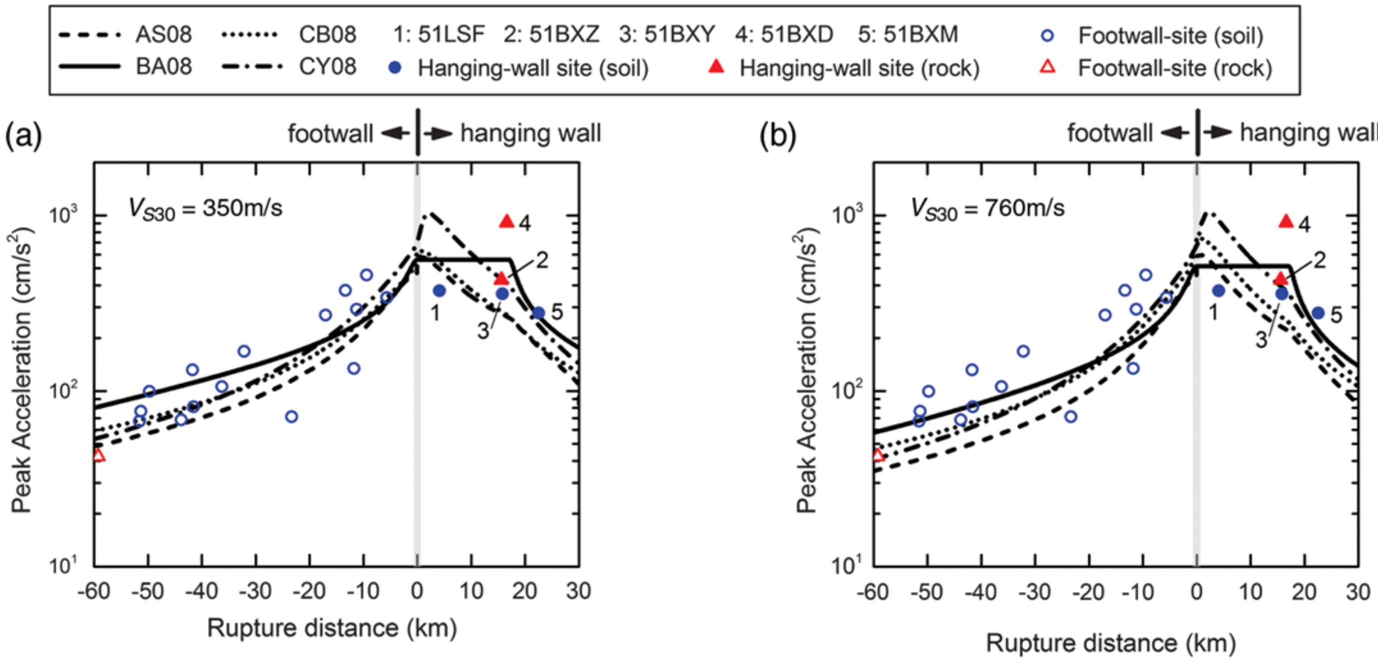

▲ **Figure 9.** Comparisons of the horizontal PGAs observed at hanging-wall and footwall sites in the Lushan earthquake with those predicted by four Next Generation Attenuation (NGA) empirical GMPEs. The predicted values were calculated with (a) $V_{S30} = 350$ m/s and (b) $V_{S30} = 760$ m/s.

for 51BXD, the residual is as high as 1.63. These results suggest the hanging-wall effect observed during the Lushan earthquake may be one of the causes for the large PGA measured at station 51BXD (1g). For the hanging-wall site 51LSF, the residual is negative, as opposed to the high residuals observed at the other four sites. This may be explained by the fact that this station is located on the transition zone between the hanging wall and footwall, which may result in an ambiguous hanging-wall effect. From the observed data, the hanging-wall effect in the Lushan earthquake seems stronger than that observed in the 2008 Wenchuan earthquake, for which the mean residual of the hanging-wall sites was just 0.28 ± 0.19 (Wang *et al.*, 2010). The difference could be linked to a possible dependence on the magnitude, dip angle, or depth of the fault rupture.

Furthermore, a comparison is made between the observed PGAs for the hanging-wall and footwall sites and the four GMPEs in NGA-West1, namely AS08 (Abrahamson and Silva, 2008), BA08 (Boore and Atkinson, 2008), CB08 (Campbell and Bozorgnia, 2008), and CY08 (Chiou and Youngs, 2008), as shown in Figure 9. As described previously, the soil and rock sites are supposed to correspond to $V_{S30} = 350$ m/s and $V_{S30} = 760$ m/s, respectively. The footwall sites are plotted using negative distance to distinguish them from the hanging-wall sites. There is good global agreement between the observed data and the models. Using the models with soil site conditions gives a slightly better agreement compared with those that take into account rock conditions (most of the data are soil sites, and there is only one rock station on the footwall). However, the observed PGA at site 51BXD is always considerably larger than of the values estimated with any of the empirical GMPEs, regardless of the site condition that is considered.

Potential Topographic Effects

A free-field strong-motion station is intended to measure ground surface motions that are not contaminated by a structural response or soil–structure interaction. In China, a code called "Specification for the construction of seismic station: strong-motion station (DB/T 17-2006)" requires free-field stations to be installed away from major structures by more than the largest dimension of that structure and away from topographic features, such as hills, ridges, and valleys, that might contaminate the ground motions. However, in western China, especially for the Lushan County region, it is not easy to find ideal free-field sites for strong-motion stations.

The surface topography can significantly affect the earthquake ground motions, as shown through an experimental and theoretical analysis (Geli *et al.*, 1988). Our objective is to attempt to understand whether topographic effects affected the free-field stations that recorded the Lushan earthquake.

Figure 10 shows the topographic profiles of four free-field stations. Station 51BXY is located on flat ground within a small valley, far from topographic slopes. However, stations 51BXM, 51LSF, and 51BXD are located either on river terraces or on the slope of steep hills, implying that the topography may have an effect on the observed ground motions. In particular, station 51BXD, which recorded the largest PGA, is located on the midslope of a small hill (a detailed description was provided by Wen *et al.* [2013] and Ren, Ji, *et al.* [2013]).

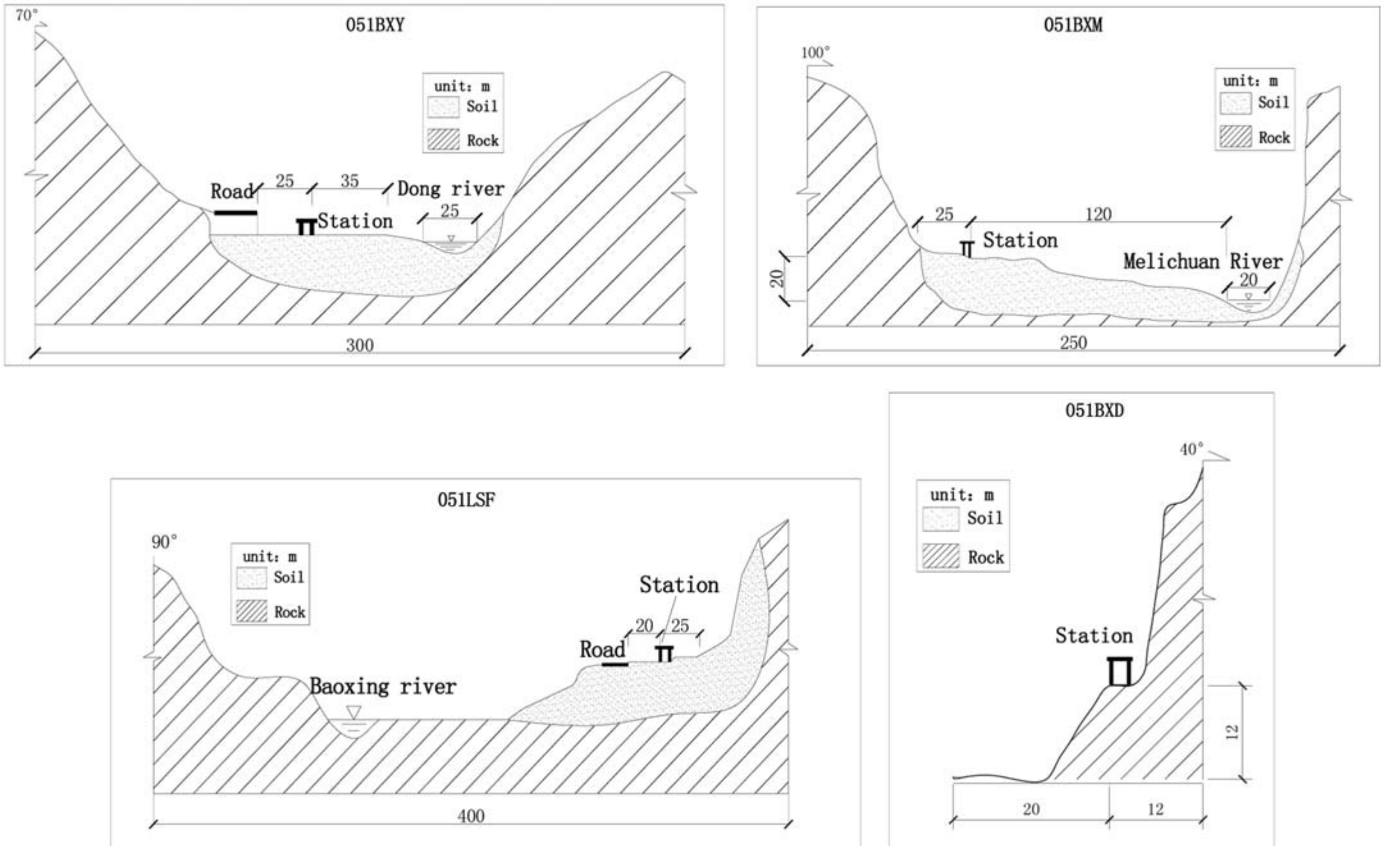

▲ **Figure 10.** Topographic profiles at the location of four near-field strong-motion stations that recorded the Lushan earthquake. The angle shown in the upper left corner of each panel denotes the azimuth (north by east).

Wen *et al.* (2013) calculated H/V spectral ratios from ambient noise recordings acquired along the slope of a hill and observed site amplification for a wide range of frequencies (3–20 Hz) in the middle of the slope. The amplitudes of the H/V peaks are approximately 4.0, 2.5, and 1.5 for frequencies of 15, 7, and 3 Hz for sites on the foothill, midhill, and uphill, respectively. A preliminary numerical simulation based on the 3D spectral element method that also supports this topographic amplification observed approximately at 8 Hz (Dai and Li, 2013). Therefore, we conclude that topographic effects combined with hanging-wall effects could explain the large PGA values recorded at station 51BXD.

CONCLUSIONS

Strong-motion observation in China has made great progress since the first recording was obtained at Xinfengjiang Dam Array in 1962. The cumulative number of strong-motion recordings is growing rapidly. The Lushan earthquake is another example of a major event producing a large number of strong-motion recordings similar to the 2008 Wenchuan earthquake. The analysis of these recordings allows us to draw the following conclusions:

1. The observed PGAs, PGVs, and PSAs are compared with the median predictions from four GMPEs in China and indicate that the data from the Lushan earthquake are consistent (considering the uncertainty linked with site conditions) with the median values predicted by the models (Huo, 1989; Yu and Wang, 2006; Lei *et al.*, 2007; Yu *et al.*, 2013). The comparison with the GMPE developed by Huo (1989) shows an overprediction for PSAs at long periods (1 and 2 s) with an epicenter distance of less than 100 km. The comparison with the GMPE (BSSA2013) developed by Boore *et al.* (2013) shows that residuals have an increasing trend with increasing distance, exhibiting low anelastic attenuation (i.e., high Q) around Lushan County, Sichuan Province, China, compared with other active regions. The observed PSAs at $T = 0.5$, 1.0, and 2.0 s are mostly lower than the median values within $R_{JB} = 100$ km, implying a low between-event residual for Lushan earthquake from the BSSA2013 GMPE.
2. In the near field, evidence of hanging-wall effects on ground motions has been shown for the Lushan earthquake based on 16 stations on the footwall and 5 stations on the hanging wall.
3. In the far field, the basin-edge effect in the Weihe basin, in addition to the amplification linked to deep sediment layers, could affect the observed data, as inferred by the SSR method based on the recordings from the mainshock of the Lushan earthquake sequence.

4. Topographic effects are not yet well understood and are not typically considered in engineering design codes or in GMPEs. Free-field stations are usually located far from topographic features, but this is not always the case. As shown by the topographic profiles, some strong-motion stations (e.g., station 51BXD) may experience a potential topographic effect. We conclude that topographic and hanging-wall effects may explain the large-amplitude recording at station 51BXD, which presented PGA values larger than 1*g*.

ACKNOWLEDGMENTS

We thank Stéphane Drouet, an anonymous reviewer, and the editor for their valuable suggestions and constructive comments, which helped us to improve the manuscript. This work was supported by the National Natural Science Fund (Numbers 51308515 and 51278473) and Nonprofit Industry Research Project of China Earthquake Administration (CEA; Number 201208014). We acknowledge Wang Weimin from the Institute of Tibetan Plateau Research of the Chinese Academy of Sciences for sharing his focal mechanism solution of the Lushan earthquake. The authors thank David M. Boore and Roger Borcherdt from the U.S. Geological Survey and Jamison Steidl from University of California, Santa Barbara, for their valuable suggestions and comments. This work also benefited from discussions of the Lushan earthquake during the 2013 COSMOS Technical Session held in Emeryville, California, U.S. on 22 November 2013. The authors also acknowledge the China Strong Motion Networks Center (CSMNC) for providing the strong-motion data from the Lushan earthquake, and all of the data included in this paper are freely available upon request from CSMNC (www.csmnc.net; last accessed January 2014).

REFERENCES

Abrahamson, N., and W. Silva (2008). Summary of the Abrahamson & Silva NGA ground-motion relations, *Earthq. Spectra* **24,** no. 1, 67–97.

Abrahamson, N. A., and P. G. Somerville (1996). Effects of the hanging wall and footwall on ground motions recorded during the Northridge earthquake, *Bull. Seismol. Soc. Am.* **86,** no. 1B, S93–S99.

Boore, D. M. (2001). Effect of baseline corrections on displacements and response spectra for several recordings of the 1999 Chi-Chi, Taiwan, earthquake, *Bull. Seismol. Soc. Am.* **91,** no. 5, 1199–1211.

Boore, D. M., and G. M. Atkinson (2008). Ground-motion prediction equations for the average horizontal component of PGA, PGV, and 5%-damped PSA at spectral periods between 0.01 s and 10.0 s, *Earthq. Spectra* **24,** no. 1, 99–138.

Boore, D. M., J. P. Stewart, E. Seyhan, and G. Atkinson (2013). NGA-West 2 equations for predicting response spectral accelerations for shallow crustal earthquakes, *PEER Report 2013/05*, Pacific Earthquake Engineering Research Center, Berkeley, California.

Campbell, K. W., and Y. Bozorgnia (2008). NGA ground motion model for the geometric mean horizontal component of PGA, PGV, PGD and 5% damped linear elastic response spectra for periods ranging from 0.01 to 10 s, *Earthq. Spectra* **24,** no. 1, 139–171.

Celebi, M., J. Prince, C. Dietel, M. Onate, and G. Chavez (1987). The culprit in Mexico City—Amplification of motions, *Earthq. Spectra* **3,** no. 2, 315–328.

Chang, T. Y., F. Cotton, Y. B. Tsai, and J. Angelier (2004). Quantification of hanging-wall effects on ground motion-some insights from the 1999 Chi-Chi earthquake, *Bull. Seismol. Soc. Am.* **94,** no. 6, 2186–2197.

China Strong Motion Networks Center (2012). *Report on Strong Earthquake Motion Recordings in China*, Vol. 16, no. 1, Earthquake Publishing Press, Beijing, China (in Chinese).

Chiou, B. S. J., and R. R. Youngs (2008). An NGA model for the average horizontal component of peak ground motion and response spectra, *Earthq. Spectra* **24,** no. 1, 173–215.

Dai, Z. J., and X. J. Li (2013). An explanation of the large PGA value of 2013 M_s 7.0 Lushan earthquake at 51BXD station through topographic analysis, *Earthq. Sci.* **26,** nos. 3/4, 199–205.

Fang, L. H., J. P. Wu, W. L. Wang, Z. Y. Lü, and C. Z. Wang (2013). Relocation of the mainshock and aftershock sequences of M_s 7.0 Sichuan Lushan earthquake, *Chin. Sci. Bull.* **58,** nos. 28/29, 3451–3459.

Geli, L., P. Y. Bard, and B. Jullien (1988). The effect of topography of earthquake ground motion: A review and new results, *Bull. Seismol. Soc. Am.* **78,** no. 1, 42–63.

Hu, Y. X., and M. Z. Zhang (1983). Attenuation of ground motion for regions with no ground motion data, *Proc. 4th Canadian Conference on Earthquake Engineering*, Vancouver, Canada, 15–17 June 1983, University of British Columbia, 485–494.

Huo, J. R. (1989). Study on the attenuation laws of strong earthquake ground motion near the source, *Doctoral dissertation*, Institute of Engineering Mechanics, China Earthquake Administration, Harbin, China (in Chinese).

Lei, J. C., M. T. Gao, and Y. X. Yu (2007). Seismic motion attenuation relations in Sichuan and adjacent areas, *Acta Seismol. Sin.* **29,** no. 5, 500–511 (in Chinese).

Li, X. J., Z. H. Zhou, M. Huang, R. Z. Wen, H. Y. Yu, D. W. Lu, Y. N. Zhou, and J. W. Cui (2008). Preliminary analysis of strong-motion recordings from the magnitude 8.0 Wenchuan China, earthquake of 12 May 2008, *Seismol. Res. Lett.* **79,** no. 6, 844–854.

Li, X. J., Z. H. Zhou, H. Y. Yu, R. Z. Wen, D. W. Lu, M. Huang, Y. N. Zhou, and J. W. Cui (2008). Strong motion observations and recordings from the great Wenchuan earthquake, *Earthq. Eng. Eng. Vib.* **7,** no. 3, 235–246.

Liu, Q. F., and X. J. Li (2009). Preliminary analysis of the hanging wall effect and velocity pulse of the 5.12 Wenchuan earthquake, *Earthq. Eng. Eng. Vib.* **8,** no. 2, 165–177.

Peng, J. B. (1992). Tectonic evolution and seismicity of Weihe fault zone, *Seismol. Geol.* **14,** no. 2, 113–120 (in Chinese).

Ren, Y. F., K. Ji, R. Z. Wen, and X. T. Huang (2013). Field survey around strong motion stations and its implications on the seismic intensity in the Lushan earthquake on April 20, 2013, *Earthq. Sci.* **26,** nos. 3/4, 241–250.

Ren, Y. F., R. Z. Wen, H. Yamanaka, and T. Kashima (2013). Site effects by generalized inversion technique using strong motion recordings of the 2008 Wenchuan earthquake, *Earthq. Eng. Eng. Vib.* **12,** no. 2, 165–184.

Ren, Y. F., R. Z. Wen, and B. F. Zhou (2011). Cataloging strong-motion recordings—An example of Wenchuan mobile strong-motion observation, *Technol. Earthq. Disaster Prev.* **6,** no. 4, 406–415 (in Chinese).

Wang, D., L. L. Xie, N. A. Abrahamson, and S. Li (2010). Comparison of strong ground motion from the Wenchuan, China, earthquake of 12 May 2008 with the Next Generation Attenuation (NGA) ground-motion models, *Bull. Seismol. Soc. Am.* **100,** no. 5B, 2381–2395.

Wang, H. Y. (2011). Amplification effects of soil sites on ground motions in the Weihe basin, *Chin. J. Geophys.* **54,** no. 1, 137–150 (in Chinese).

Wang, W. M., J. L. Hao, and Z. X. Yao (2013). Preliminary result for rupture process of Apr. 20, 2013, Lushan earthquake, Sichuan, China, *Chin. J. Geophys.* **56,** no. 4, 1412–1417 (in Chinese).

Wen, R. Z., Y. F. Ren, W. H. Qi, T. Lu, Z. Y. Yang, Z. D. Shan, and Y. L. Wang (2013). Maximum acceleration recording from Lushan earthquake on April 20, 2013, *J. Southwest Jiaotong University* **48,** no. 5, 783–791 (in Chinese).

Xie, J. J., X. J. Li, Z. P. Wen, and C. Q. Wu (2014). Near-source vertical and horizontal strong ground motion from the 20 April 2013 M_w 6.8 Lushan earthquake in China, *Seismol. Res. Lett.* **85,** no. 1, 23–33.

Xu, X. W., X. Z. Wen, Z. J. Han, G. H. Chen, C. Y. Li, W. J. Zheng, S. M. Zhang, Z. Q. Ren, C. Xu, X. B. Tan, Z. Y. Wei, M. M. Wang, J. J. Ren, Z. T. He, and M. J. Liang (2013). Lushan M_s 7.0 earthquake: A blind reserve-fault event, *Chin. Sci. Bull.* **58,** nos. 28/29, 3437–3443.

Yu, Y. X., and S. Y. Wang (2006). Attenuation relations for horizontal peak ground acceleration and response spectrum in eastern and western China, *Technol. Earthq. Disaster Prev.* **1,** no. 3, 206–217 (in Chinese).

Yu, Y. X., S. Y. Li, and L. Xiao (2013). Development of ground motion attenuation relations for the new seismic hazard map of China, *Technol. Earthq. Disaster Prev.* **8,** no. 1, 24–33 (in Chinese).

Ruizhi Wen
Yefei Ren
Key Laboratory of Earthquake Engineering and Engineering Vibration
Institute of Engineering Mechanics
China Earthquake Administration
No. 29 Xuefu Road
Harbin, Heilongjiang 150080
People's Republic of China
ruizhi@iem.ac.cn
renyefei@iem.ac.cn